ADVANCES IN ATMOSPHERIC SCIENCES, VOL. 38, MAY 2021, 817–830

• Original Paper •

CMIP6 Evaluation and Projection of Temperature and Precipitation over China

Xiaoling YANG[1,2], Botao ZHOU[*1,2], Ying XU[3], and Zhenyu HAN[3]

[1]*Collaborative Innovation Center on Forecast and Evaluation of Meteorological Disasters/Key Laboratory of Meteorological Disaster*, *Ministry of Education/Joint International Research Laboratory of Climate and Environment Change*, *Nanjing University of Information Science and Technology*, *Nanjing* 210044, *China*

[2]*School of Atmospheric Sciences*, *Nanjing University of Information Science and Technology*, *Nanjing* 210044, *China*

[3]*National Climate Center*, *China Meteorological Administration*, *Beijing* 100081, *China*

(Received 16 October 2020; revised 23 December 2020; accepted 5 January 2021)

ABSTRACT

This article evaluates the performance of 20 Coupled Model Intercomparison Project phase 6 (CMIP6) models in simulating temperature and precipitation over China through comparisons with gridded observation data for the period of 1995–2014, with a focus on spatial patterns and interannual variability. The evaluations show that the CMIP6 models perform well in reproducing the climatological spatial distribution of temperature and precipitation, with better performance for temperature than for precipitation. Their interannual variability can also be reasonably captured by most models, however, poor performance is noted regarding the interannual variability of winter precipitation. Based on the comprehensive performance for the above two factors, the "highest-ranked" models are selected as an ensemble (BMME). The BMME outperforms the ensemble of all models (AMME) in simulating annual and winter temperature and precipitation, particularly for those subregions with complex terrain but it shows little improvement for summer temperature and precipitation. The AMME and BMME projections indicate annual increases for both temperature and precipitation across China by the end of the 21st century, with larger increases under the scenario of the Shared Socioeconomic Pathway 5/Representative Concentration Pathway 8.5 (SSP585) than under scenario of the Shared Socioeconomic Pathway 2/Representative Concentration Pathway 4.5 (SSP245). The greatest increases of annual temperature are projected for higher latitudes and higher elevations and the largest percentage-based increases in annual precipitation are projected to occur in northern and western China, especially under SSP585. However, the BMME, which generally performs better in these regions, projects lower changes in annual temperature and larger variations in annual precipitation when compared to the AMME projections.

Key words: CMIP6 evaluation and projection, temperature, precipitation, ensemble

Citation: Yang, X. L., B. T. Zhou, Y. Xu, and Z.-Y. Han, 2021: CMIP6 evaluation and projection of temperature and precipitation over China. *Adv. Atmos. Sci.*, **38**(5), 817−830, https://doi.org/10.1007/s00376-021-0351-4.

Article Highlights:

- Most CMIP6 models perform reasonably well in reproducing the spatial patterns and interannual variability of annual temperature and precipitation.
- BMME outperforms AMME for simulating annual and winter temperature and precipitation, particularly in subregions with complex terrain.
- BMME projects lower (higher) increases in annual temperature (precipitation) compared to the AMME projection over subregions with large changes.

1. Introduction

The Coupled Model Intercomparison Project (CMIP) has been coordinating simulations conducted by international modeling groups since the 1990s, with the aim of improving the performance of climate models and enhancing the scientific understanding of the climate system. This project has become a major tool for climate science, and remarkable progress has been achieved for global climate models (GCMs) (Eyring et al., 2016; Stouffer et al., 2017). At present, the CMIP phase 6 (CMIP6) is being carried out

* Corresponding author: Botao ZHOU
Email: zhoubt@nuist.edu.cn

(Simpkins, 2017). Compared with previous phases, the number of experiments that have been designed in the CMIP6 is the largest. The physical processes of the CMIP6 models are more complicated, and their resolutions are enhanced (Eyring et al., 2016; Zhou et al., 2019). These CMIP6 simulations will support climate change research in the upcoming several years (Zhou et al., 2019).

Temperature and precipitation are essential indicators for climate change. In the past few years, many research efforts have been devoted to model evaluations and projections of temperature and precipitation over China within the CMIP phase 5 (CMIP5) framework. The evaluations indicated that the CMIP5 models, in general, show reasonable performance in capturing the geographical distributions of surface temperature and precipitation (e.g., Xu and Xu, 2012b; Guo et al., 2013; Huang et al., 2013; Kumar et al., 2014; Sun et al., 2015; Jiang et al., 2016). Compared with CMIP phase 3 (CMIP3), the CMIP5 performances were improved for temperature while there was little performance change for precipitation (Kumar et al., 2014; Sun et al., 2015; Jiang et al., 2016). Some common biases, such as topography-related cold biases, underestimations of southeast-northwest precipitation gradients, and overestimations of the magnitudes of the interannual variability of temperature and precipitation, are also present in the CMIP5 simulations (Su et al., 2013; Chen et al., 2014; Bao and Feng, 2016; Jiang et al., 2016). For the CMIP5 projections, an overall warming of temperature and a general increase in precipitation are projected over China by the end of the 21st century under the Representative Concentration Pathways (RCPs), further noting the expectation of larger changes to occur for higher RCPs (e.g., Xu and Xu, 2012a; Su et al., 2013; Chen and Frauenfeld, 2014; Hu et al., 2015; Wu et al., 2015; Tan et al., 2016; Zhang et al., 2017).

In general, these findings improve our knowledge of the simulation abilities of CMIP5 models and future climate changes under the RCP scenarios. Questions naturally arise regarding the performance of CMIP6 models for the climate in China and how China's climate would change in the context of the new CMIP6 scenarios (i.e., Shared Socioeconomic Pathways, SSPs), which represents the motivation of this study. Some recent studies have begun to evaluate and project the East Asian monsoon climate using CMIP6 data (Chen et al., 2020; Ha et al., 2020; Jiang et al., 2020; Nie et al., 2020; Zhu et al., 2020; Xin et al., 2020) and have indicated a general improvement of CMIP6 models compared with CMIP5 models regarding simulations of both mean temperature and precipitation as well as extreme temperature and precipitation events. For example, a smaller spread is observed among CMIP6 models as well as a weaker cold bias of temperature and a weaker underestimation of the southeast–northwest precipitation gradient (Chen et al., 2020; Jiang et al., 2020). However, more detailed regional analysis is still needed. In addition, some previous CMIP studies have used the multimodel ensemble for projecting the climate of China (e.g., Xu and Xu, 2012a; Chen and Frauenfeld, 2014; Zhou et al., 2014; Tian et al., 2015; Wu et al., 2015; Wang et al., 2017) and some have used the optimal model ensemble (e.g., Chen and Sun, 2009, 2013; Chen et al., 2011; Hu et al., 2015; Zhou et al., 2018a; Rao et al., 2019). Determining the nature of the differences between the optimal model ensemble and the multimodel ensemble for CMIP6 projections of climate over China is also an area of concern in this study. Addressing this topic will aid in the understanding of uncertainties in the projections.

2. Data and methods

Simulation data from 20 CMIP6 models (Table 1) are used in this study. For each model, the near-surface air temperature and precipitation results from the historical simulation and the SSP245 and SSP585 experiments are employed. The SSP245 and SSP585 reflect a set of alternative futures of social development and greenhouse gas emission. The SSP245 represents the combined scenario of a moderate socio-economic development path (i.e., SSP2) with the medium-low radiation forcing which peaks at 4.5 W m^{-2} by 2100. The SSP585 represents the combined scenario of a high energy-intensive, socio-economic developmental path (i.e., SSP5) with strong radiative forcing which peaks at 8.5 W m^{-2} by 2100 (O'Neill et al., 2016; Riahi et al., 2017).

The observed temperature and precipitation data of CN05.1 with a resolution of 0.25°×0.25° (Wu and Gao, 2013) are used to validate the performance of the CMIP6 models. For convenience, all data are converted to the same 1°×1° grid using a bilinear interpolation scheme before analysis. As recommended by the CMIP6, the period 1995–2014 is used as the reference period for the evaluation and projection. The ensemble in this study is calculated with the same weight. The statistical significance is examined by the Student's *t*-test.

A Taylor diagram (Taylor, 2001) is used to evaluate spatial distributions of temperature and precipitation over China. This diagram provides a concise statistical summary of how well a simulated pattern matches an observed pattern in terms of the spatial correlation coefficient (SCC), the root-mean-square error (RMSE), and the ratio of variances. The interannual variability of the simulations relative to the observations is assessed by the interannual variability skill score (IVS) (Gleckler et al., 2008; Scherrer, 2011), which is calculated as

$$\mathrm{IVS} = \left(\frac{\mathrm{STD_m}}{\mathrm{STD_o}} - \frac{\mathrm{STD_o}}{\mathrm{STD_m}}\right)^2,$$

where $\mathrm{STD_m}$ and $\mathrm{STD_o}$ are the standard deviations of the simulation and observation, respectively. IVS is a symmetric variability statistic that is used to measure the similarity of interannual variation between the simulation and observation. A smaller IVS value indicates a better simulation of interannual variability.

To quantitatively examine regional differences, following Zhou et al. (2014), we divide China into eight subre-

gions: Northeast China (NEC; 39°–54°N, 119°–134°E), North China (NC; 36°–46°N, 111°–119°E), East China (EC; 27°–36°N, 116°–122°E), Central China (CC; 27°–36°N, 106°–116°E), Northwest China (NWC; 36°–46°N, 75°–111°E), Tibetan Plateau (SWC1; 27°–36°N, 77°–106°E), Southwest China (SWC2; 22°–27°N, 98°–106°E), and South China (SC; 20°–27°N, 106°–120°E) (see Fig. 1), all of which are based on administrative boundaries and societal and geographical conditions (National Report Committee, 2007).

3. Evaluations

3.1. *Climatology and interannual variability*

Figures 2a–f show the climatological spatial distributions of annual, winter (December to February, DJF), and summer (June to August, JJA) temperatures from observations and the ensemble simulation of all models (AMME), respectively. In general, the AMME simulated spatial patterns approximate those of the observations. However, relat-

Table 1. Basic information for the CMIP6 models used in this study.

ID	Model name	Institution and country	Atmospheric resolution (lon×lat: number of grids, L: vertical levels)
1	ACCESS-CM2	Commonwealth Scientific and Industrial Research Organization, Australian Research Council Centre of Excellence for Climate System Science, Australia	192×144, L85
2	ACCESS-ESM1-5	Commonwealth Scientific and Industrial Research Organization, Australia	192×145, L38
3	BCC-CSM2-MR	Beijing Climate Center, China	320×160, L46
4	CanESM5	Canadian Centre for Climate Modelling and Analysis, Canada	128 × 64, L49
5	CESM2	National Center for Climate Research, USA	288 × 192, L32
6	CESM2-WACCM	National Center for Climate Research, USA	288 × 192, L70
7	EC-Earth3	EC-Earth Consortium, Europe	512 × 256, L91
8	EC-Earth3-Veg	EC-Earth Consortium, Europe	512 × 256, L91
9	FGOALS-g3	Chinese Academy of Sciences, China	180 × 80, L26
10	GFDL-CM4	National Oceanic and Atmospheric Administration, Geophysical Fluid Dynamics Laboratory, USA	288 × 180, L33
11	GFDL-ESM4	National Oceanic and Atmospheric Administration, Geophysical Fluid Dynamics Laboratory, USA	288 × 180, L49
12	INM-CM4-8	Institute for Numerical Mathematics, Russia	180 × 120, L21
13	INM-CM5-0	Institute for Numerical Mathematics, Russia	180 × 120, L73
14	IPSL-CM6A-LR	Institute Pierre Simon Laplace, France	144 × 143, L79
15	MIROC6	Atmosphere and Ocean Research Institute, The University of Tokyo, Japan	256 × 128, L81
16	MPI-ESM1-2-HR	Max Planck Institute for Meteorology, Germany	384 × 192, L95
17	MPI-ESM1-2-LR	Max Planck Institute for Meteorology, Alfred Wegener Institute, Germany	192× 96, L47
18	MRI-ESM2-0	Meteorological Research Institute, Japan	320 ×160, L80
19	NorESM2-LM	NorESM Climate modeling Consortium, Norway	144 × 96, L32
20	NorESM2-MM	NorESM Climate modeling Consortium, Norway	288 × 192, L32

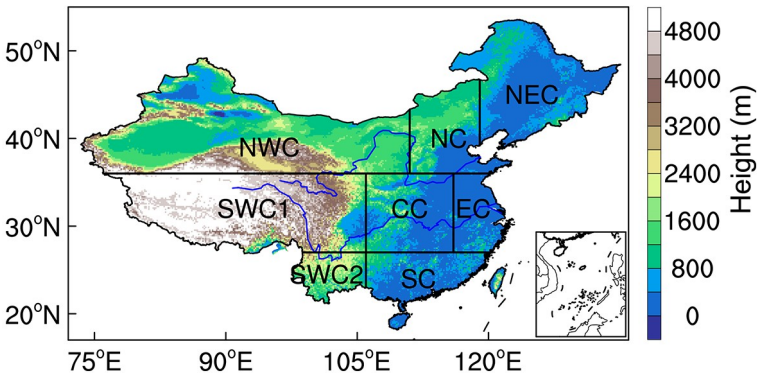

Fig. 1. Domains and topography (shading, units: m) of eight sub-regions in China. NEC: Northeast China; NC: North China; EC: East China; CC: Central China; NWC: Northwest China; SWC1: Tibetan Plateau; SWC2: Southwest China; SC: South China.

ive to the observations, a general underestimation of annual temperature is noted over most of China in the AMME simulation. The most pronounced cold bias is located in the Tibetan Plateau (Fig. 2g). This phenomenon was also present in the CMIP3 and CMIP5 simulations as revealed by previous studies (Jiang et al., 2005; Xu and Xu, 2012a; Jiang et al., 2016). For winter (Fig. 2h) and summer (Fig. 2i) temperatures, there are notable warm biases in parts of northern China, in addition to the cold bias in the Tibetan Plateau.

For observed precipitation (Figs. 3a–c), the annual, winter, and summer precipitation amounts decrease from the southeast coast to the northwest areas. These spatial patterns are captured by the AMME simulation (Figs. 3d–f) but with overall wet biases (Figs. 3g–i). The wet bias for annual precipitation appears in most parts of northern and western China, particularly on the northern and southern flanks of the Tibetan Plateau (Fig. 3g), which was also reported for the CMIP3 and CMIP5 simulations (Jiang et al., 2005; Xu and Xu, 2012a; Jiang et al., 2016). Compared with the CMIP5, the wet bias in the CMIP6 models was observed to be smaller (Jiang et al., 2020; Zhu et al., 2020). The spatial distributions of wet biases for winter precipitation resemble that for annual precipitation, but with larger bias magnitudes (Fig. 3h). Besides the wet bias, dry biases are also notable for summer precipitation in parts of Northwest China and East China (Fig. 3i).

Figure 4 shows the Taylor diagrams for annual, winter, and summer temperature and precipitation over China as simulated by the 20 CMIP6 models and AMME against the observations. The azimuthal position of the model point indicates the SCC between the simulated and observed patterns. The distance from the reference point (REF) to the model point indicates the normalized RMSE of the simulation relative to the observation. The radial distance from the origin to the model point indicates the ratio of standard deviations between the simulation and observation. The overall model biases are excluded in this diagram. Clearly, the CMIP6 models show better performance for temperature than for precipitation. For temperature, regardless of whether winter, summer, or annual mean values are used, the SCCs between the simulations and observations are all greater than 0.9, the RMSEs of the simulations relative to the observations are generally below 0.5, and the ratios of variances to the observations are close to 1 for most models. These results indicate

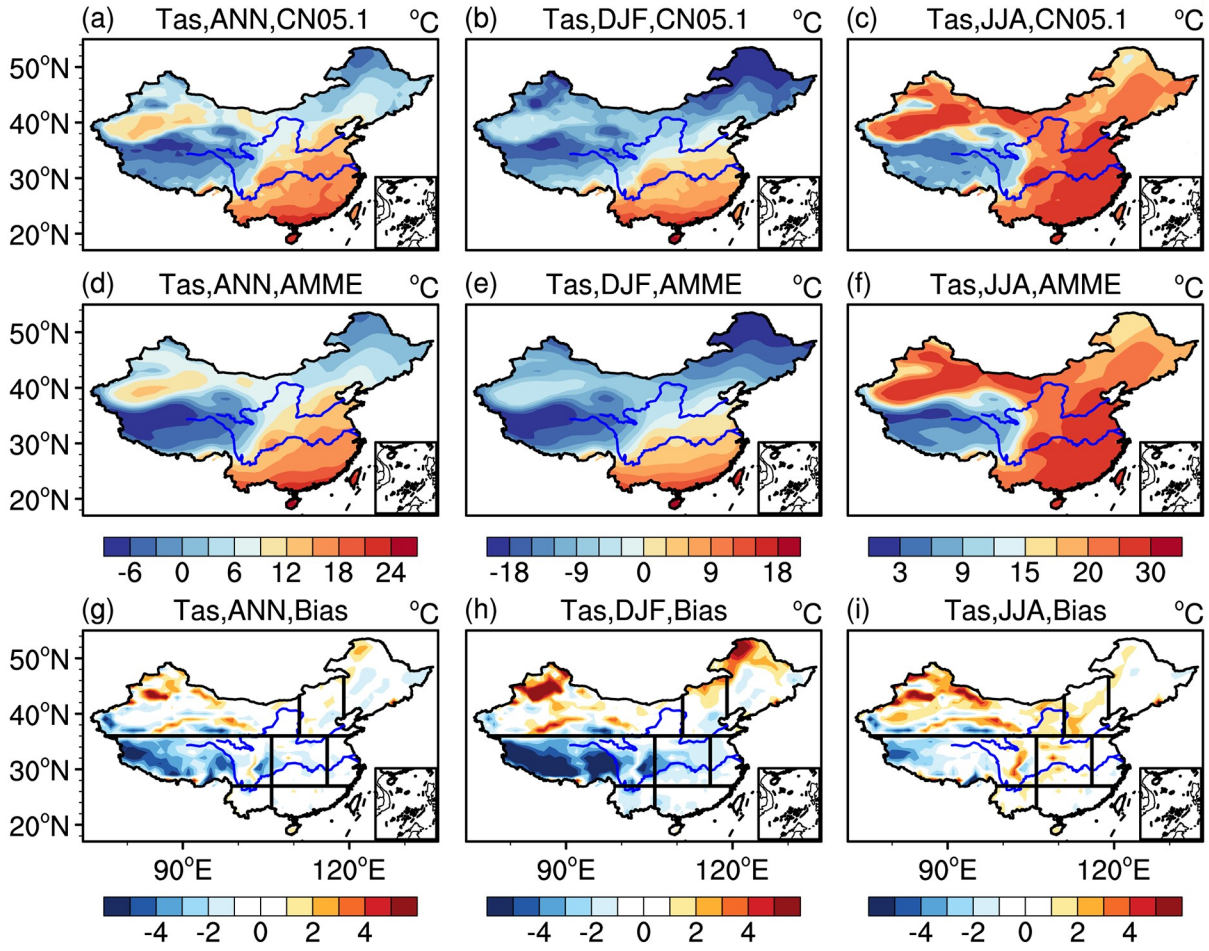

Fig. 2. Spatial distributions of (a–c) observed temperature (units: °C), (d–f) AMME simulated temperature (units: °C), and (g–i) AMME simulation biases from the observation (simulation minus observation, units: °C) for the period 1995–2014. The panels from the left to right side are for annual (ANN), winter (DJF), and summer (JJA), respectively. The black lines in (g)–(i) show the boundary of subregions. Note that the scales of color bars are different.

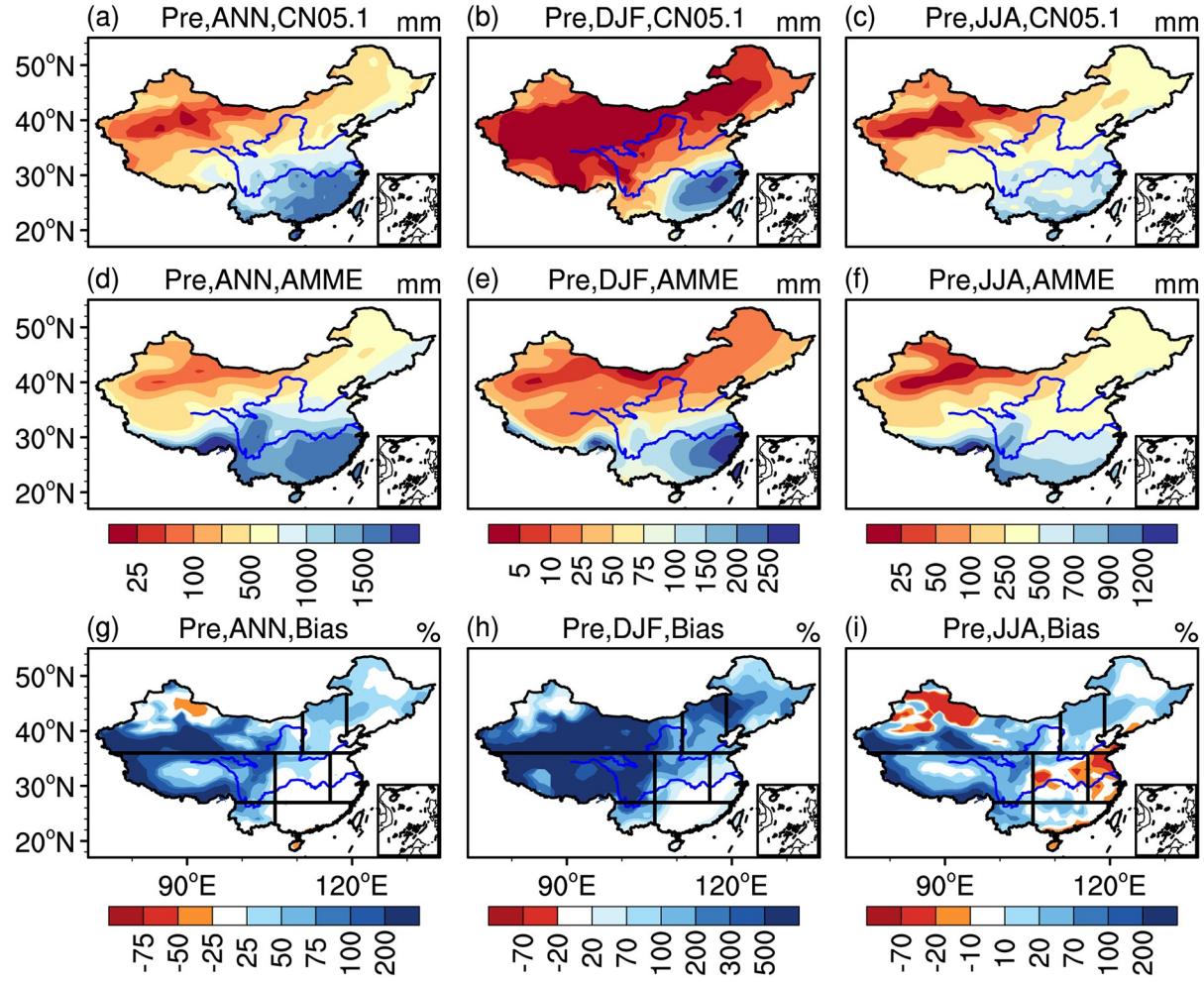

Fig. 3. Spatial distributions of (a–c) observed precipitation (units: mm), (d–f) AMME simulated precipitation (units: mm), and (g–i) AMME simulation biases from the observation ((simulation minus observation)/observation, units: %) for the period 1995–2014. The panels from the left to right side are for annual (ANN), winter (DJF), and summer (JJA), respectively. The black lines in (g)–(i) show the boundary of subregions. Note that the scales of color bars are different.

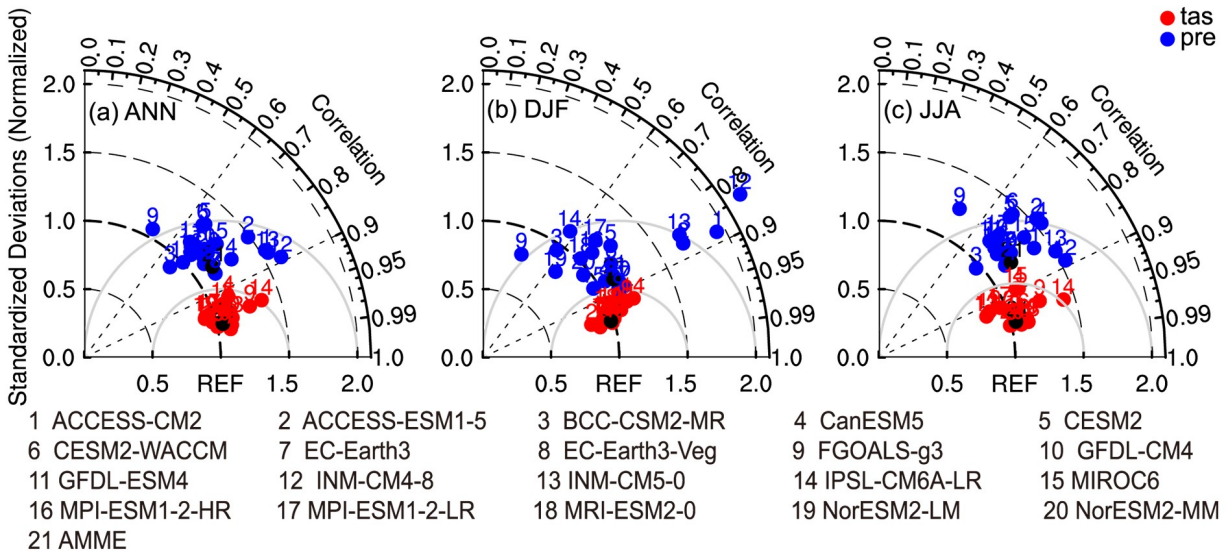

Fig. 4. Taylor diagrams of (a) annual (ANN), (b) winter (DJF), and (c) summer (JJA) temperature (red dots; units: °C) and precipitation (blue dots; units: mm) over China for the period 1995–2014. The black dot in each panel represents AMME.

that the CMIP6 models effectively capture the climatological distributions in terms of annual, summer, and winter temperatures.

Compared with temperature, the SCCs for precipitation over China are relatively lower and the RMSEs are relatively higher. Specifically, the SCCs and RMSEs are mainly in the range of 0.6–0.9 (still statistically significant) and 0.5–1, respectively. In addition, the ratios of variances mostly lie between 1 and 1.5. Overall, the simulations of most models are reliable for the spatial patterns of annual, summer, and winter precipitation, although the variances are overestimated.

Figure 5 presents the IVS values of the simulations for the interannual variability of annual, winter, and summer temperature and precipitation over China. In this study, the IVS values were first calculated in each grid of China and then averaged. For temperature (Fig. 5a), the IVS values are below 1.5 for all models except for CanESM5 which shows a value of 4.0 in summer. This suggests that the CMIP6 models can reasonably reproduce the observed interannual variability of annual, winter, and summer temperature. In comparison, the model performances for the interannual variability of annual and winter temperatures are better than their performances in summer. For precipitation (Fig. 5b), though the IVS values are larger than those for temperature, the relatively low IVS values in annual mean and summer imply a reasonable reproduction of the observed interannual variability by the CMIP6 models. It also reflects the dominant contribution of summer precipitation to annual precipitation (Sui et al., 2013). There is a large range for the winter IVS values, which vary from 7.1 to 62.9 and are much larger than those of annual mean and summer. This result indicates large inconsistencies among the models and poor simulations for the interannual variability of winter precipitation.

According to Gleckler et al. (2008), the rankings for all models that considered the three factors of the Taylor diagram and the interannual variability skill score are summarized in Fig. 6. This figure depicts the overall performance of individual models. A smaller ranking value indicates a better performing model. The rankings for the Taylor diagram are the average of the rankings of SCC, RMSE, and ratio of variance. On the whole, the AMME outperforms its ensemble members in a comprehensive manner. For a given individual model, the performance ranks are somewhat different for different metrics. Considering the comprehensive performance for both spatial patterns and IVS, the relatively "highest-ranked" and "lowest-ranked" models are selected based on Fig. 6 and listed in Table 2. For these "highest-ranked" and "lowest-ranked" models, their comprehensive performances (arithmetic average of the rankings for Taylor Diagram and IVS) rank in the top three and bottom three among all models, respectively. Note that ACCESS-ESM1-5 and CESM2-WACCM (ACCESS-ESM1-5 and CESM2) show the same ranking for annual (summer) precipitation.

Some studies have shown that increasing the model resolution is an effective way to improve the performance of model simulations (Yao et al., 2017; Zhou et al., 2018b; Bador et al., 2020), thus we examine the relationships between the model performances and resolutions. The analyses show that the comprehensive performances of the models and their resolutions are significantly correlated. The correlation coefficients are 0.50 and 0.81 for annual and summer temperatures, respectively. The comprehensive performance of the models for winter precipitation also show a significant correlation of 0.65 with their resolutions, which is consistent with the previous finding that model resolution influ-

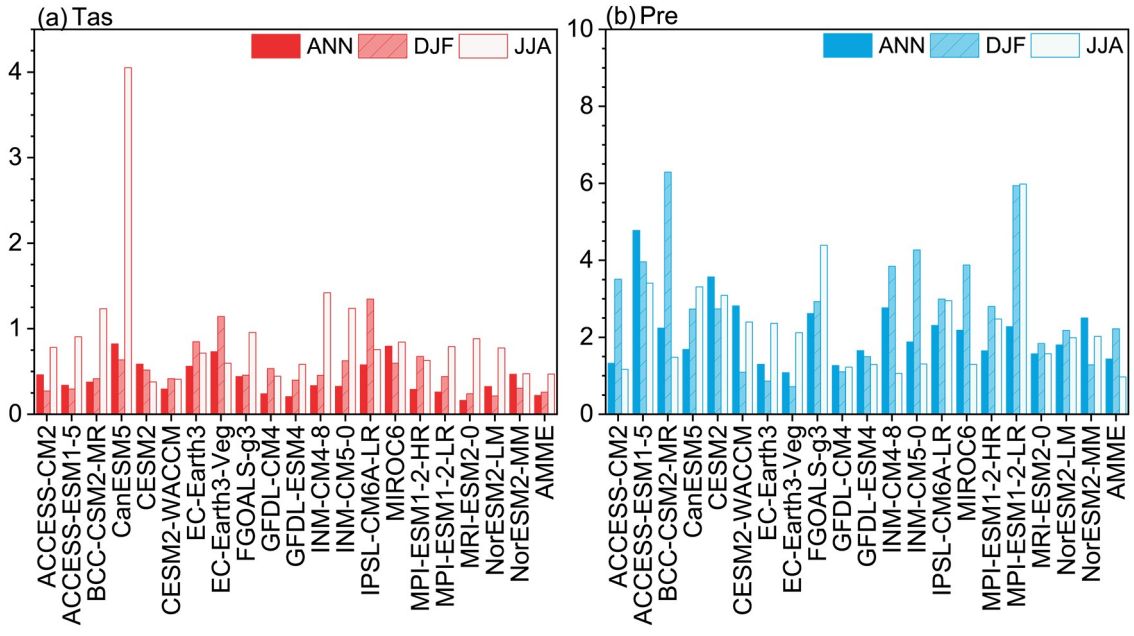

Fig. 5. Interannual variability skill score (IVS) of the CMIP6 models for annual (ANN), winter (DJF), and summer (JJA) (a) temperature and (b) precipitation over China. Note that the IVS for winter precipitation is divided by 10.

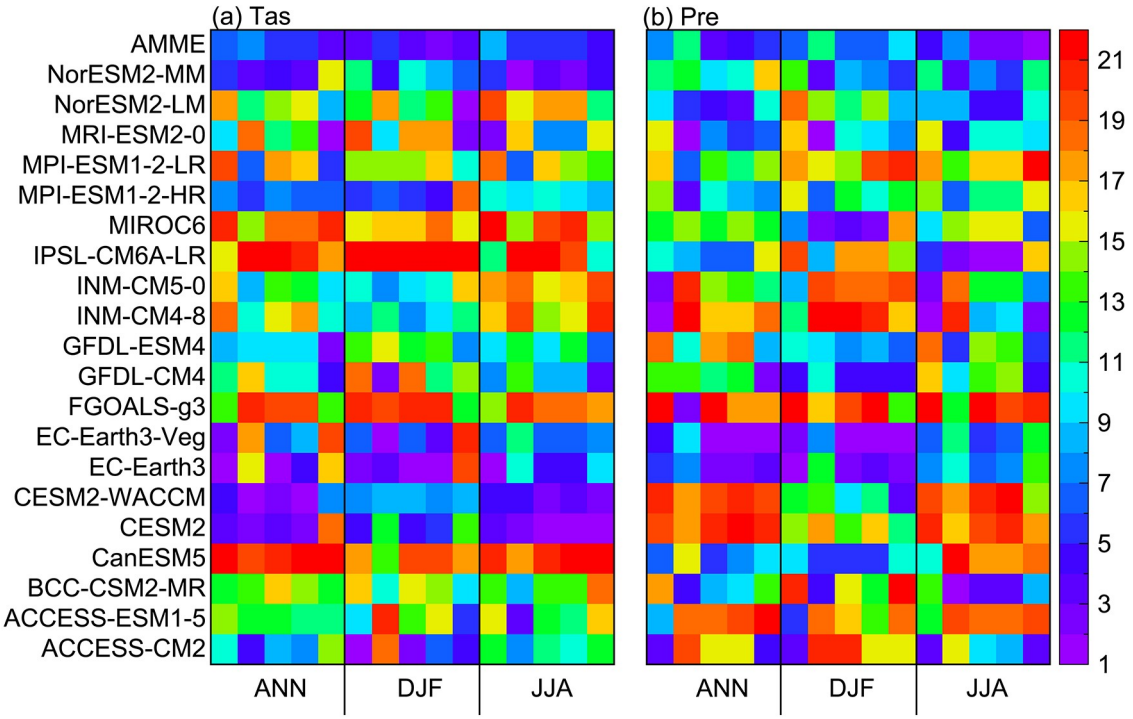

Fig. 6. Portrait diagram of the rankings of model performance for annual (ANN), winter (DJF), and summer (JJA) (a) temperature (units: °C) and (b) precipitation (units: mm). The colors in the label bar indicate the rankings. A smaller ranking number indicates a better model performance. Columns from the left to the right side in each group show the rankings of the SCC, ratio of variances, and RMSE, mean rankings of the three factors in the Taylor diagram, and IVS rankings, respectively.

Table 2. Highest and lowest ranking models selected for the ensembles for annual (ANN), winter (DJF), and summer (JJA) temperature and precipitation.

	ANN		DJF		JJA	
	Highest ranked models	Lowest ranked models	Highest ranked models	Lowest ranked models	Highest ranked models	Lowest ranked models
Tas	CESM2-WACCM GFDL-ESM4 MPI-ESM1-2-HR	CanESM5 IPSL-CM6A-LR MIROC6	ACCESS-CM2 CESM2-WACCM NorESM2-MM	CanESM5 IPSL-CM6A-LR MIROC6	CESM2 CESM2-WACCM NorESM2-MM	CanESM5 FGOALS-g3 INM-CM5-0
Pre	EC-Earth3 EC-Earth3-Veg MRI-ESM2-0	ACCESS-ESM1-5 CESM2 CESM2-WACCM FGOALS-g3	EC-Earth3 EC-Earth3-Veg GFDL-CM4	MPI-ESM1-2-LR INM-CM4-8 INM-CM5-0	ACCESS-CM2 BCC-CSM2-MR INM-CM4-8	ACCESS-ESM1-5 CESM2 FGOALS-g3 MPI-ESM1-2-LR

ences the simulation of winter precipitation in China (Gao et al., 2006; Jiang et al., 2016, 2020).

3.2. *Comparison of different ensemble simulations*

Figure 7 shows the spatial distributions of the biases from the "highest-ranked" model ensemble (hereafter BMME) and the "lowest-ranked" model ensemble (hereafter WMME) for annual temperature and precipitation. Compared with the AMME simulation (Fig. 2g), the cold bias over the Tibetan Plateau is reduced in the BMME simulation (Fig. 7a) and augmented in the WMME simulation (Fig. 7b). The regionally averaged BMME, AMME, and WMME biases in SWC1 are −1.3°C, −2.0°C, and −4.3°C, respectively (Fig. 8a). From a seasonal perspective, the performance of the BMME for winter temperature is better than that of the AMME and WMME simulations over SWC1, CC, EC, SC, and SWC2 (Fig. 8c). However, due to an overall warm bias, the BMME does not perform better than the AMME in simulating summer temperature but does indicate a smaller spread (Fig. 8e).

For annual precipitation, the wet biases in the AMME simulation (Fig. 3g) decrease in the BMME simulation (Fig. 7c) and increase in the WMME simulation (Fig. 7d). When regionally averaged, the percentage-based wet biases over NWC, SWC1, NC, and NEC are 199%, 191%, 45%, and 28% respectively for the WMME simulation. These decrease to 136%, 147%, 40%, and 32% for the AMME simula-

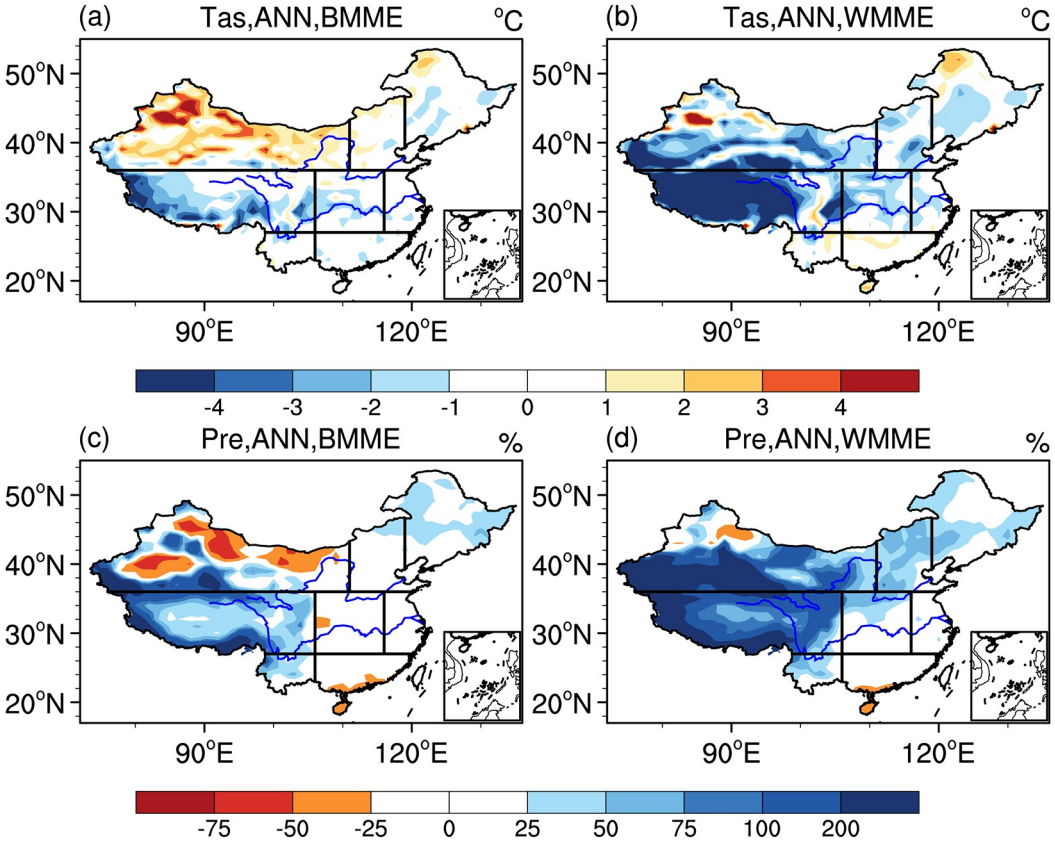

Fig. 7. Spatial distributions of (a, c) BMME and (b, d) WMME simulation biases for annual (a, b) temperature (simulation minus observation, units: °C) and (c, d) precipitation [(simulation minus observation)/observation, units: %]. The black lines show the boundary of subregions.

tion; the wet biases further reduce to 39%, 96%, 4%, and 23% in the BMME simulation, respectively (Fig. 8b). Similar results are obtained for the simulation of winter precipitation (Fig. 8d). Nevertheless, there is no improvement in the BMME simulation for summer precipitation over subregions except for EC, NWC, and NEC when compared to the AMME and WMME simulations, although the model spread is reduced.

In short, the BMME generally shows better performance than the AMME and WMME in reproducing the spatial patterns of annual and winter temperature and precipitation, particularly in subregions with complex terrain. Similarly, regardless of whether for annual, winter, or summer temperature (precipitation), the BMME presents the smallest IVS values, followed by the AMME and then by the WMME. The IVS values for annual, winter, and summer temperature (precipitation) over China are 0.1 (0.9), 0.2 (8.3), and 0.3 (1.0) from the BMME simulation, 0.2 (1.4), 0.3 (22.2), and 0.5 (1.0) from the AMME simulation, and 0.6 (2.4), 0.7 (43.4), and 1.1 (1.4) from the WMME simulation, respectively.

4. Projected Changes

Figure 9 displays the temporal evolution of the projected changes in annual temperature and precipitation over China under SSP245 and SSP585 from the AMME, BMME, and WMME. Similar to the CMIP5 projection (e.g., Xu and Xu, 2012a; Chen and Sun, 2013; Tian et al., 2015; Tan et al., 2016), an increasing trend toward the end of the 21st century is projected for annual temperature and precipitation, with larger increases under SSP585 than under SSP245. Relative to the reference period of 1995–2014, the increases in annual temperature (precipitation) by the end of the 21st century that are projected by the AMME are 2.7°C (17%) under SSP245 and 5.4°C (30%) under SSP585. Compared with the AMME projection, the BMME (WMME) projects a smaller (larger) increase in temperature and a larger (smaller) increase in precipitation under each scenario. At the end of the 21st century under SSP245 and SSP585, the BMME projected increases in annual temperature (precipitation) are 2.4°C and 4.8°C (24% and 45%), respectively, and those projected by the WMME are 3.3°C and 7.0°C (13% and 25%), respectively.

Figure 10 further illustrates the spatial distributions of the projected changes in annual temperature under SSP245 and SSP585 by the end of the 21st century. The annual temperature is projected to increase across China, with much stronger warming under SSP585. The greatest warming under SSP585 occurs at higher latitudes and higher elevations of China such as in NEC, NWC, and SWC1. In contrast, the warming is comparable across subregions under

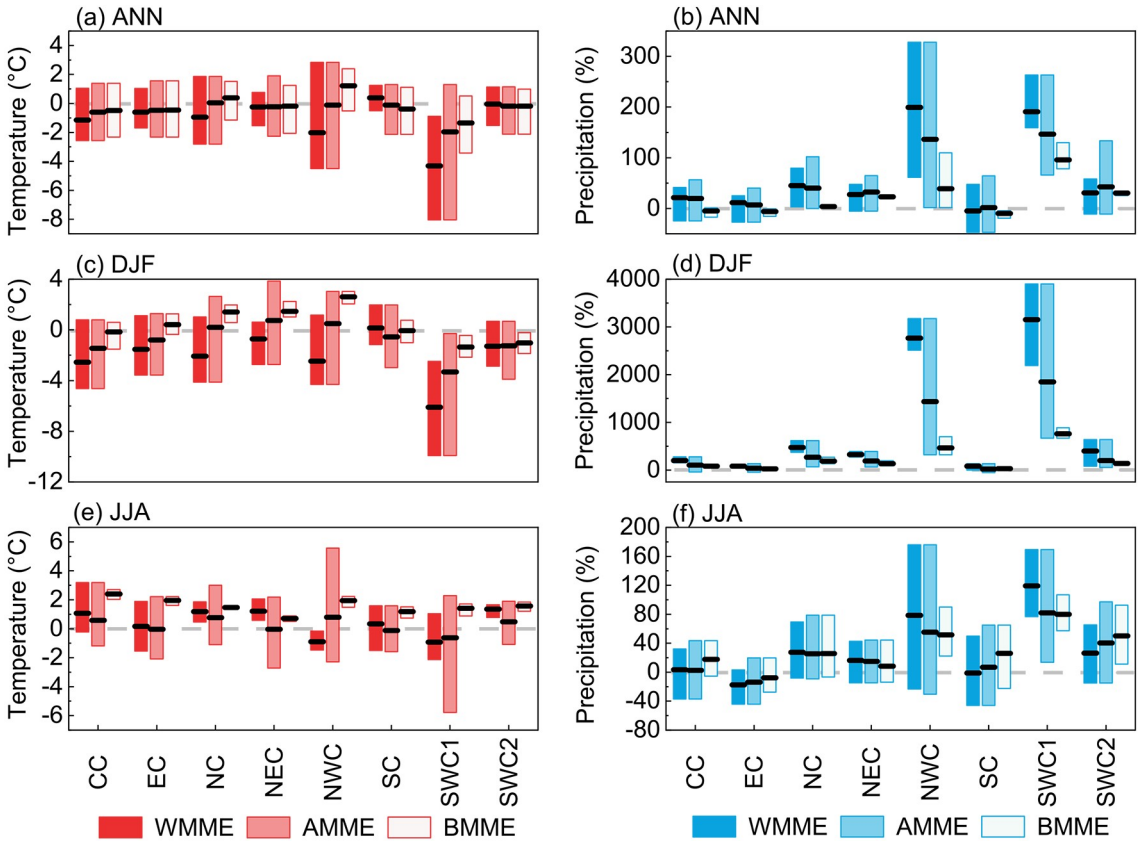

Fig. 8. Biases of the BMME, AMME, and WMME simulations for annual (ANN), winter (DJF), and summer (JJA) temperature (left panel, units: °C) and precipitation (right panel, units: %) in eight subregions of China. Boxes indicate the range of biases from the ensemble models and the black lines show the ensemble mean values. Note that the vertical scales are different.

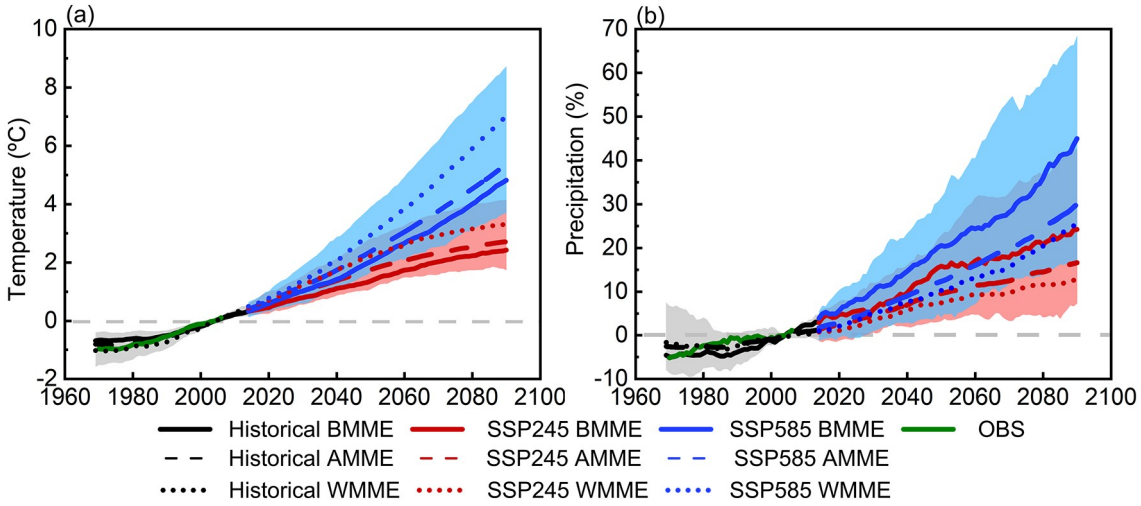

Fig. 9. Time series of annual (a) temperature (units: °C) and (b) precipitation (units: %) anomalies (relative to 1995–2014) over China for the observation (green), historical simulation (black), SSP245 (red), and SSP585 (blue). Solid, dashed, and dotted lines indicate the BMME, AMME, and WMME simulations, respectively. The shadings show the AMME ensemble spread. The time series are smoothed with a 20-yr running mean filter.

SSP245. Of particular interest, the warming magnitudes under both scenarios gradually increase from the BMME projection to the AMME projection and then to the WMME projection, which may be associated with different climate sensitivities in the models and/or regional land-atmosphere feedbacks (Zhou and Chen, 2015; Tokarska et al., 2020; Zelinka, et al., 2020). When regionally averaged over subregions (Fig. 11a), the BMME projects an increase of 2.1°C

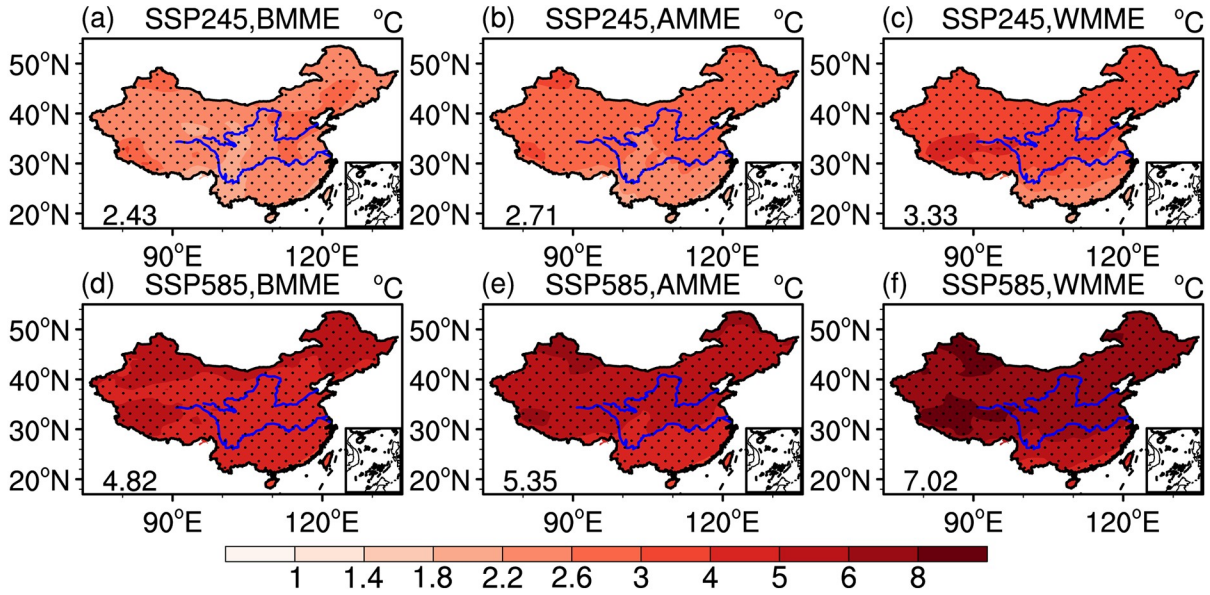

Fig. 10. Projected changes in annual temperature (units: °C) under (a–c) SSP245 and (d–f) SSP585 over the period 2081–2100 relative to the reference period 1995–2014 from (a, d) BMME, (b, e) AMME, and (c, f) WMME. Black solid dots indicate those grids with statistically significant changes at the 95% level. The values in the lower-left corners represent the changes averaged over China.

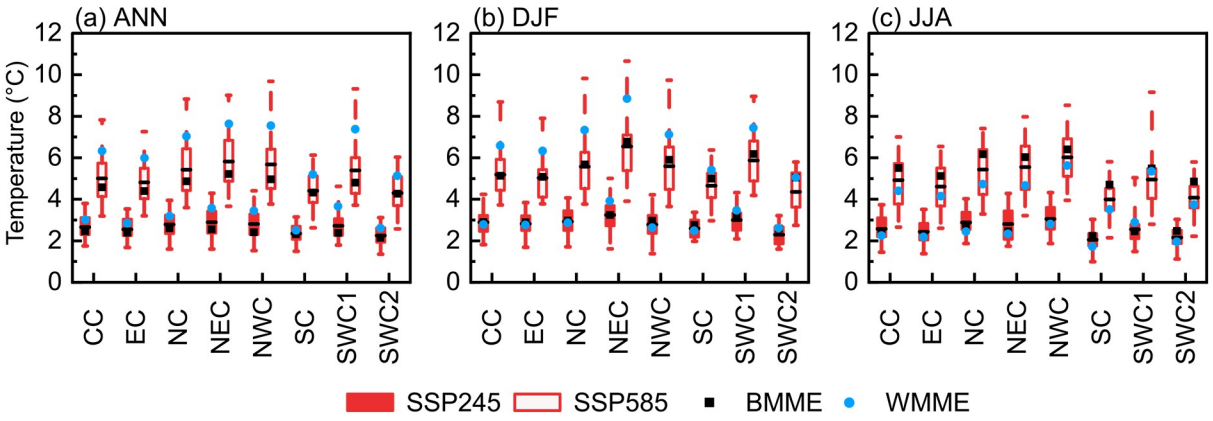

Fig. 11. Projected changes in (a) annual (ANN), (b) winter (DJF), and (c) summer (JJA) temperature (units: °C) under SSP245 and SSP585 over the period 2081–2100 relative to the reference period 1995–2014. Boxes indicate the interquartile model spread (i.e., 25th and 75th quantiles), horizontal lines indicate the AMME values, and whiskers show the AMME ensemble ranges. Black rectangles and blue solid dots represent the BMME and WMME values, respectively.

(SWC2) to 2.6°C (NC) under SSP245. The increases projected by the AMME range from 2.3°C (SWC2) to 2.9°C (NEC), which are slightly higher than the BMME projection in each subregion. Those projected by the WMME are in a range of 2.5°C (SC) to 3.7°C (SWC1), which are the highest among the three ensemble projections. Under SSP585, the greatest changes that exceed 5°C as projected by the AMME, occur in NEC (5.8°C), NWC (5.7°C), NC (5.4°C), and SWC1 (5.4°C). The magnitudes of increase over these subregions decrease to 5.2°C, 5.0°C, 4.9°C, and 4.8°C, respectively, in the BMME projection, while they increase to 7.6°C, 7.6°C, 7.1°C, and 7.4°C in the WMME projection, respectively. From a seasonal perspective, the AMME and WMME generally project larger increases in winter temperature than in summer temperature by the end of the 21st century under SSP585. The BMME projected increases in winter temperature are also larger than those of summer temperature in NEC, SWC1, SWC2, and SC, but it is reversed in NWC, NC, CC, and EC (Figs. 11b, c). In addition, the BMME projected increases in winter temperature are generally higher than the AMME projection and lower than the WMME projection (Fig. 11b); the increases in summer temperature from the BMME projection are larger than the AMME and WMME projections (Fig. 11c). Moreover, the spreads of the projections for annual, winter, and summer temperature from the BMME ensemble members are narrowed, compared with the projections from the AMME and WMME ensemble members (Figure not shown).

The spatial distributions of the projected percentage changes for annual precipitation under SSP245 and SSP585

are shown in Fig. 12. By the end of the 21st century, the annual precipitation is projected to increase uniformly across the country, and the magnitude of the increase is greater under SSP585 than under SSP245. Moreover, the projected percentage increases are larger in northern China than in southern China. The largest increase is anticipated over western China due to the drier climate toward the north and northwest areas, which is consistent with the CMIP5 projection (Zhou et al., 2014). Although the three ensembles show resemblances in their spatial distributions for the projected changes, salient differences exist in the magnitudes among the projections. For instance, compared with the AMME projection under SSP585 (Fig. 12e), the percentage increases of annual precipitation over northern and western China are enhanced in the BMME projection, whereas they are reduced in the WMME projection. There are no obvious differences among the three ensembles for the precipitation projections over eastern China.

Figure 13a summarizes the projected percentage changes in annual precipitation over subregions. Under SSP585, annual precipitation amounts, as projected by the BMME in NWC, NC, NEC, and SWC1 (i.e., northern and western regions of China) are expected to increase by 81%, 43%, 35%, and 32% at the end of the 21st century, respectively, which are larger than those of the AMME projection (45%, 30%, 25%, 29%, respectively) and the WMME projection (33%, 21%, 20%, 29%, respectively). Note that the historical simulation of the BMME shows the smallest biases from the observation in these subregions (Fig. 8b). The case for the SSP245 scenario is generally similar but with smaller magnitudes of percentage increase. Seasonal changes in precipitation in winter (Fig. 13b) and summer (Fig. 13c), as projected from the three ensembles under SSP585, generally approximate those of annual precipitation in the above subregions. We also notice that the magnitudes of percentage increases are much more pronounced in winter than in summer. For example, in the NWC, NC, and NEC subregions, the increases of winter precipitation from the BMME projection are 262%, 145%, and 106%, compared with 28%, 30%, and 29% increases for summer, respectively. This result suggests a relatively larger contribution to annual precipitation change from the increased winter precipit-

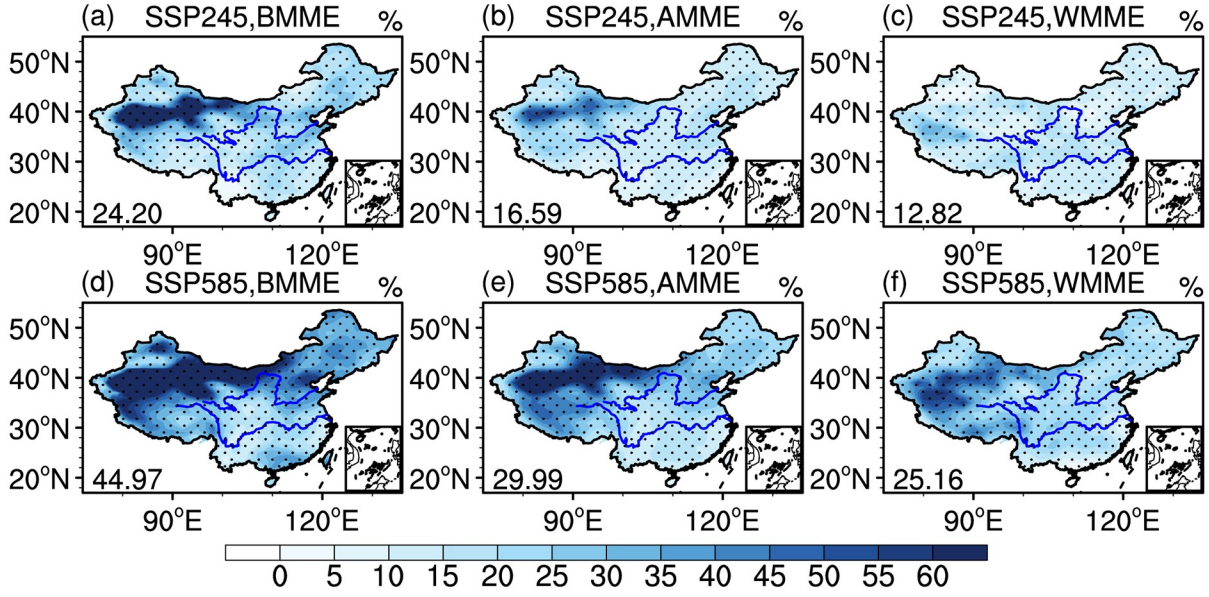

Fig. 12. Same as in Fig. 10, but for annual precipitation (units: %).

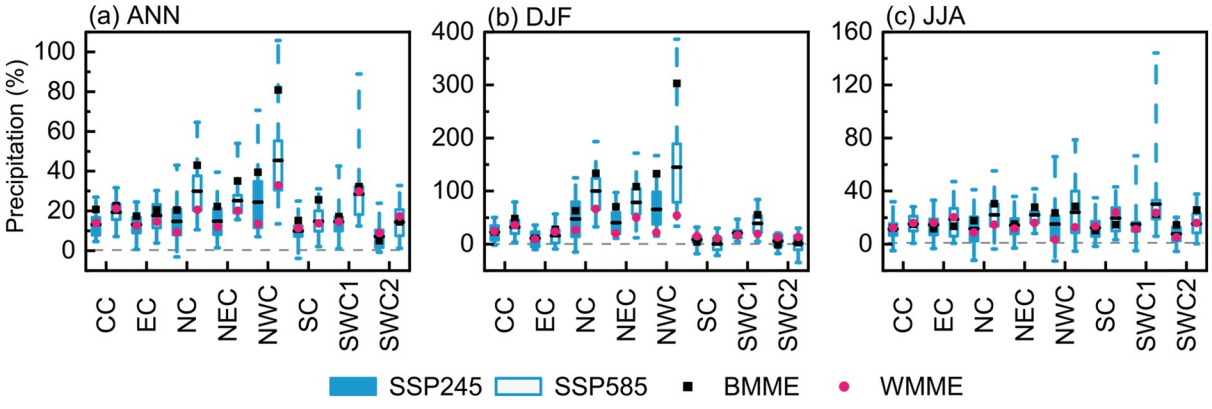

Fig. 13. Same as in Fig. 11, but for precipitation (units: %). Note that the vertical scales are different.

ation. However, because of the different climatology of seasonal precipitation, it may not necessarily reflect the absolute changes in precipitation values. A similar seasonal change but with smaller magnitudes of percentage increase is noted in CC. The opposite seasonal pattern is projected in SC, where the projected percentage increases in summer are larger than those in winter. The cases for other subregions (e.g., SWC2 and EC) are diverse for the three ensemble projections.

5. Conclusion

In this study, we evaluated the performance of 20 CMIP6 models in simulating temperature and precipitation over China from the perspective of spatial pattern and interannual variability. Generally, the CMIP6 models show a good ability to capture the climatological distributions of temperature and precipitation, with better performance for temperature than for precipitation. The interannual variability of temperature and precipitation can be reasonably reproduced by most models, although poor performance is shown for that of winter precipitation. Comparative analysis conducted by Jiang et al. (2020) also indicated that the performances have improved from CMIP5 to CMIP6 for climatological temperature and precipitation, but show little improvement for their interannual variability. Based upon the comprehensive model performance regarding both spatial patterns and interannual variability, the ensembles of the "highest-ranked" models (BMME), the "lowest-ranked" models (WMME), and all models (AMME) are determined. It is worth noting that the relevant model rankings could differ for other applications (e.g., climate extremes). The differences among the aforementioned three ensembles for simulations and projections of temperature and precipitation over China are examined. The main findings are summarized below:

(1) The BMME outperforms the AMME and WMME for the simulation of annual and winter temperature and precipitation, particularly in those subregions with complex terrain. Nevertheless, there is no salient improvement for summer temperature or precipitation over most of the subregions.

(2) The three ensembles all project increased temperature and precipitation over China by the end of the 21st century, accompanied by larger increases under SSP585 than under SSP245. For the SSP585 scenario, the greatest warming is projected to occur at higher latitudes and at higher elevations of China (such as in NEC, NWC, and SWC1). The largest percentage-based increase in annual precipitation is anticipated in northern and western China.

(3) The three ensembles project different magnitudes of increase in temperature and precipitation. By the end of the 21st century under SSP585, the warming of annual temperature is the lowest in the BMME projection, which increases successively in the AMME and WMME projections. The BMME projected percentage increases in annual, summer, and winter precipitation over northern and western China are larger than those projected from the AMME and WMME.

Acknowledgements. We acknowledge the World Climate Research Program's Working Group on Coupled Modeling and thank the climate modeling groups for producing and sharing their model outputs. This research was jointly supported by the National Key Research and Development Program of China (2018YFA0606301) and the National Natural Science Foundation of China (42025502, 41991285, 42088101).

REFERENCES

Bador, M., and Coauthors, 2020: Impact of higher spatial atmospheric resolution on precipitation extremes over land in Global Climate Models. *J. Geophys. Res.*, **125**, e2019JD032184, https://doi.org/10.1029/2019JD032184.

Bao, J. W., and J. M. Feng, 2016: Intercomparison of CMIP5 simulations of summer precipitation, evaporation, and water vapor transport over Yellow and Yangtze River basins. *Theor. Appl. Climatol.*, **123**, 437–452, https://doi.org/10.1007/s00704-014-1349-y.

Chen, H. P., and J. Q. Sun, 2009: How the "best" models project the future precipitation change in China. *Adv. Atmos. Sci.*, **26**, 773–782, https://doi.org/10.1007/s00376-009-8211-7.

Chen, H. P., and J. Q. Sun, 2013: Projected change in East Asian summer monsoon precipitation under RCP scenario. *Meteorol. Atmos. Phys.*, **121**, 55–77, https://doi.org/10.1007/s00703-013-0257-5.

Chen, H. P., J. Q. Sun, W. Q. Lin, and H. W. Xu, 2020: Comparison of CMIP6 and CMIP5 models in simulating climate extremes. *Science Bulletin*, **65**, 1415–1418, https://doi.org/10.1016/j.scib.2020.05.015.

Chen, L., and O. W. Frauenfeld, 2014: A comprehensive evaluation of precipitation simulations over China based on CMIP5 multimodel ensemble projections. *J. Geophys. Res.*, **119**, 5767–5786, https://doi.org/10.1002/2013JD021190.

Chen, W. L., Z. H. Jiang, and L. Li, 2011: Probabilistic projections of climate change over China under the SRES A1B scenario using 28 AOGCMs. *J. Climate*, **24**, 4741–4756, https://doi.org/10.1175/2011JCLI4102.1.

Chen, X. C., Y. Xu, C. H. Xu, and Y. Yao, 2014: Assessment of precipitation simulations in China by CMIP5 multi-models. *Progressus Inquisitiones de Mutatione Climatis*, **10**, 217–225, https://doi.org/10.3969/j.issn.1673-1719.2014.03.011. (in Chinese with English abstract)

Eyring, V., S. Bony, G. A. Meehl, C. A. Senior, B. Stevens, R. J. Stouffer, and K. E. Taylor, 2016: Overview of the Coupled Model Intercomparison Project Phase 6 (CMIP6) experimental design and organization. *Geoscientific Model Development*, **9**, 1937–1958, https://doi.org/10.5194/gmd-9-1937-2016.

Gao, X. J., Y. Xu, Z. C. Zhao, J. S. Pal, and F. Giorgi, 2006: On the role of resolution and topography in the simulation of East Asia precipitation. *Theor. Appl. Climatol.*, **86**, 173–185, https://doi.org/10.1007/s00704-005-0214-4.

Gleckler, P. J., K. E. Taylor, and C. Doutriaux, 2008: Performance metrics for climate models. *J. Geophys. Res.*, **113**, D06104, https://doi.org/10.1029/2007JD008972.

Guo, Y., W. J. Dong, F. M. Ren, Z. C. Zhao, and J. B. Huang, 2013: Assessment of CMIP5 simulations for China annual

average surface temperature and its comparison with CMIP3 simulations. *Progressus Inquisitiones de Mutatione Climatis*, **9**, 181–186, https://doi.org/10.3969/j.issn.1673-1719.2013.03.004. (in Chinese with English abstract)

Ha, K. J., S. Moon, A. Timmermann, and D. Kim, 2020: Future changes of summer monsoon characteristics and evaporative demand over Asia in CMIP6 simulations. *Geophys. Res. Lett.*, **47**, e2020GL087492, https://doi.org/10.1029/2020GL087492.

Hu, Q., D. B. Jiang, and G. Z. Fan, 2015: Climate change projection on the Tibetan Plateau: Results of CMIP5 models. *Chinese Journal of Atmospheric Sciences*, **39**(2), 260–270, https://doi.org/10.3878/j.issn.1006-9895.1406.13325. (in Chinese with English abstract)

Huang, D. Q., J. Zhu, Y. C. Zhang, and A. N. Huang, 2013: Uncertainties on the simulated summer precipitation over Eastern China from the CMIP5 models. *J. Geophys. Res.*, **118**, 9035–9047, https://doi.org/10.1002/jgrd.50695.

Jiang, D. B., H. J. Wang, and X. M. Lang, 2005: Evaluation of East Asian climatology as simulated by seven coupled models. *Adv. Atmos. Sci.*, **22**, 479–495, https://doi.org/10.1007/BF02918482.

Jiang, D. B., Z. P. Tian, and X. M. Lang, 2016: Reliability of climate models for China through the IPCC Third to Fifth Assessment Reports. *International Journal of Climatology*, **36**, 1114–1133, https://doi.org/10.1002/joc.4406.

Jiang, D. B., D. Hu, Z. P. Tian, and X. M. Lang, 2020: Differences between CMIP6 and CMIP5 models in simulating climate over China and the East Asian monsoon. *Adv. Atmos. Sci.*, **37**, 1102–1118, https://doi.org/10.1007/s00376-020-2034-y.

Kumar, D., E. Kodra, and A. R. Ganguly, 2014: Regional and seasonal intercomparison of CMIP3 and CMIP5 climate model ensembles for temperature and precipitation. *Climate Dyn.*, **43**, 2491–2518, https://doi.org/10.1007/s00382-014-2070-3.

National Report Committee, 2007: *China's National Assessment Report on Climate Change*. Science Press, Beijing, 148 pp. (in Chinese)

Nie, S. P., S. W. Fu, W. H. Cao, and X. L. Jia, 2020: Comparison of monthly air and land surface temperature extremes simulated using CMIP5 and CMIP6 versions of the Beijing Climate Center climate model. *Theor. Appl. Climatol.*, **140**, 487–502, https://doi.org/10.1007/s00704-020-03090-x.

O'Neill, B. C., and Coauthors, 2016: The Scenario Model Intercomparison Project (ScenarioMIP) for CMIP6. *Geoscientific Model Development*, **9**, 3461–3482, https://doi.org/10.5194/gmd-9-3461-2016.

Rao, X. Q., X. Lu, and W. J. Dong, 2019: Evaluation and projection of extreme precipitation over Northern China in CMIP5 models. *Atmosphere*, **10**, 691, https://doi.org/10.3390/atmos10110691.

Riahi, K., and Coauthors, 2017: The shared socioeconomic pathways and their energy, land use, and greenhouse gas emissions implications: An overview. *Global Environmental Change*, **42**, 153–168, https://doi.org/10.1016/j.gloenvcha.2016.05.009.

Scherrer, S. C., 2011: Present-day interannual variability of surface climate in CMIP3 models and its relation to future warming. *International Journal of Climatology*, **31**, 1518–1529, https://doi.org/10.1002/joc.2170.

Simpkins, G., 2017: Progress in climate modelling. *Nature Climate Change*, **7**, 684–685, https://doi.org/10.1038/nclimate3398.

Stouffer, R. J., V. Eyring, G. A. Meehl, S. Bony, C. Senior, B. Stevens, and K. E. Taylor, 2017: CMIP5 scientific gaps and recommendations for CMIP6. *Bull. Amer. Meteor. Soc.*, **98**, 95–105, https://doi.org/10.1175/BAMS-D-15-00013.1.

Su, F. G., X. L. Duan, D. L. Chen, Z. C. Hao, and L. Cuo, 2013: Evaluation of the global climate models in the CMIP5 over the Tibetan Plateau. *J. Climate*, **26**, 3187–3208, https://doi.org/10.1175/JCLI-D-12-00321.1.

Sui, Y., D. B. Jiang, and Z. P. Tian, 2013: Latest update of the climatology and changes in the seasonal distribution of precipitation over China. *Theor. Appl. Climatol.*, **113**, 599–610, https://doi.org/10.1007/s00704-012-0810-z.

Sun, Q. H., C. Y. Miao, and Q. Y. Duan, 2015: Comparative analysis of CMIP3 and CMIP5 global climate models for simulating the daily mean, maximum, and minimum temperatures and daily precipitation over China. *J. Geophys. Res.*, **120**, 4806–4824, https://doi.org/10.1002/2014JD022994.

Tan, J. L., Z. H. Jiang, and T. T. Ma, 2016: Projections of future surface air temperature change and uncertainty over China based on the Bayesian model averaging. *Acta Meteorologica Sinica*, **74**, 583–597, https://doi.org/10.11676/qxxb2016.044. (in Chinese with English abstract)

Taylor, K. E., 2001: Summarizing multiple aspects of model performance in a single diagram. *J. Geophys. Res.*, **106**, 7183–7192, https://doi.org/10.1029/2000JD900719.

Tian, D., Y. Guo, Y., and W. J. Dong, 2015: Future changes and uncertainties in temperature and precipitation over China based on CMIP5 models. *Adv. Atmos. Sci.*, **32**, 487–496, https://doi.org/10.1007/s00376-014-4102-7.

Tokarska, K. B., M. B. Stolpe, S. Sippel, E. M. Fischer, C. J. Smith, F. Lehner, and R. Knutti, 2020: Past warming trend constrains future warming in CMIP6 models. *Science Advances*, **6**, eaaz9549, https://doi.org/10.1126/sciadv.aaz9549.

Wang, Y. J., B. T. Zhou, D. H. Qin, J. Wu, R. Gao, and L. C. Song, 2017: Changes in mean and extreme temperature and precipitation over the arid region of northwestern China: Observation and projection. *Adv. Atmos. Sci.*, **34**, 289–305, https://doi.org/10.1007/s00376-016-6160-5.

Wu, J., and X. J. Gao, 2013: A gridded daily observation dataset over China region and comparison with the other datasets. *Chinese Journal of Geophysics*, **56**, 1102–1111, https://doi.org/10.6038/cjg20130406.(inChinesewithEnglishabstract). (in Chinese with English abstract)

Wu, J., B. T. Zhou, and Y. Xu, 2015: Response of precipitation and its extremes over China to warming: CMIP5 simulation and projection. *Chinese Journal of Geophysics*, **58**, 461–473, https://doi.org/10.1002/cjg2.20187.

Xin, X. G., T. W. Wu, J. Zhang, J. C. Yao, and Y. J. Fang, 2020: Comparison of CMIP6 and CMIP5 simulations of precipitation in China and the East Asian summer monsoon. *International Journal of Climatology*, **40**, 6423–6440, https://doi.org/10.1002/joc.6590.

Xu, C. H., and Y. Xu, 2012a: The projection of temperature and precipitation over China under RCP scenarios using a CMIP5 multi-model ensemble. *Atmos. Ocean. Sci. Lett.*, **5**, 527–533, https://doi.org/10.1080/16742834.2012.11447042.

Xu, Y., and C. H. Xu, 2012b: Preliminary assessment of simulations of climate changes over China by CMIP5 multi-models. *Atmos. Ocean. Sci. Lett.*, **5**, 489–494, https://doi.org/10.1080/16742834.2012.11447041.

Yao, J. C., T. J. Zhou, Z. Guo, X. L. Chen, L. W. Zou, and Y. Sun, 2017: Improved performance of high-resolution atmospheric models in simulating the East Asian summer monsoon rain belt. *J. Climate*, **30**, 8825–8840, https://doi.org/10.1175/JCLI-D-16-0372.1.

Zelinka, M. D., T. A. Myers, D. T. McCoy, S. Po-Chedley, P. M. Caldwell, P. Ceppi, S. A. Klein, and K. E. Taylor, 2020: Causes of higher climate sensitivity in CMIP6 Models. *Geophys. Res. Lett.*, **47**, e2019GL085782, https://doi.org/10.1029/2019GL085782.

Zhang, X. Z., X. X. Li, X. C. Xu, and L. J. Zhang, 2017: Ensemble projection of climate change scenarios of China in the 21st century based on the preferred climate models. *Acta Geographica Sinica*, **72**, 1555–1568, https://doi.org/10.11821/dlxb201709002. (in Chinese with English abstract)

Zhou, B. T., H. Q. Z. Wen, Y. Xu, L. C. Song, and X. B. Zhang, 2014: Projected changes in temperature and precipitation extremes in China by the CMIP5 multimodel ensembles. *J. Climate*, **27**, 6591–6611, https://doi.org/10.1175/JCLI-D-13-00761.1.

Zhou, B. T., Y. Xu, and Y. Shi, 2018a: Present and future connection of Asian-Pacific Oscillation to large-scale atmospheric circulations and East Asian rainfall: Results of CMIP5. *Climate Dyn.*, **50**, 17–29, https://doi.org/10.1007/s00382-017-3579-z.

Zhou, T. J., and X. L. Chen, 2015: Uncertainty in the 2°C warming threshold related to climate sensitivity and climate feedback. *J. Meteor. Res.*, **29**, 884–895, https://doi.org/10.1007/s13351-015-5036-4.

Zhou, T. J., and Coauthors, 2018b: A review of East Asian summer monsoon simulation and projection: Achievements and problems, opportunities and challenges. *Chinese Journal of Atmospheric Sciences*, **42**, 902–934, https://doi.org/10.3878/j.issn.1006-9895.1802.17306. (in Chinese with English abstract)

Zhou, T. J., L. W. Zou, and X. L. Chen, 2019: Commentary on the Coupled Model Intercomparison Project Phase 6 (CMIP6). *Climate Change Research*, **15**, 445–456, https://doi.org/10.12006/j.issn.1673-1719.2019.193. (in Chinese with English abstract)

Zhu, H. H., Z. H. Jiang, J. Li, W. Li, C. X. Sun, and L. Li, 2020: Does CMIP6 inspire more confidence in simulating climate extremes over China? *Adv. Atmos. Sci.*, **37**, 1119–1132, https://doi.org/10.1007/s00376-020-9289-1.